Available online at www.sciencedirect.com
ScienceDirect
Acta Materialia 55 (2007) 4567–4583
Acta MATERIALIA
www.elsevier.com/locate/actamat

Effects of initial orientation, sample geometry and friction on anisotropy and crystallographic orientation changes in single crystal microcompression deformation: A crystal plasticity finite element study

D. Raabe *, D. Ma, F. Roters

Max-Planck-Institut für Eisenforschung, Max-Planck-Strasse 1, 40237 Düsseldorf, Germany

Received 19 January 2007; received in revised form 12 April 2007; accepted 13 April 2007
Available online 4 June 2007

Abstract

The study presents crystal plasticity finite element simulations of cylindrical Cu single crystal micropillar compression tests. The aim is to study the influence of the stability of the initial crystal orientation, sample geometry (diameter-to-length ratio) and friction on the anisotropy and crystallographic orientation changes during such tests. Initial anisotropy (initial orientation) has a strong influence on the evolution of crystallographic orientation changes and also, to a minor extent, on the sample shape during compression. Pronounced orientation changes occur at an early stage of compression (at engineering strains of 0.2), entailing as a rule a large orientation spread within the initially uniformly oriented sample. A non-zero friction has a stabilizing effect on the course of the compression test even in cases where strong orientation changes occur. The evolution of orientation changes during compression is in part due to rigid body rotations (shape inclination due to buckling) rather than exclusively to crystallographic reorientation. Orientations that are crystallographically unstable and non-symmetric during compression tend to entail shape instability of the pillars at an earlier stage than observed for more stable cases.

Keywords: Column; Pillar; Compression; Orientation; Misorientation

1. Introduction and motivation

Mechanical size effects discovered recently during microscale compression tests of crystalline metallic single crystals [1] are currently attracting great attention. The main experimental observation is that the mechanical properties observed during such tests become remarkably different compared with bulk specimens when the sample dimensions of the pillars approach the micrometer scale. Uchic et al. [1] tested three different materials: Ni, Ni_3Al–1% Ta and a Ni-based superalloy. By mapping the engineering stress–strain curves during microscale compression the authors observed that the yield stresses dramatically increased as the diameters of the test pillars decreased. The group of Nix and Greer [2,3] performed similar tests on gold pillars but used two different sample fabrication methods. The authors found a similarly significant flow stress increase as in Ref. [1], and proposed that a dislocation starvation effect could have been responsible for this. Their hypothesis suggests that due to the small dimensions of the specimens the dislocations that are present at the onset of plastic deformation leave these specimens before dislocations can multiply: this results in dislocation starvation. The authors propose that if this state is reached, very high stresses would be required to nucleate new dislocations, either at the sample surface or in the bulk of the crystal, leading to the observed near-theoretical strengths. Similar observations were reported by Dimiduk et al. [4] and Volkert and Lilleoden [5].

Afrin and Ngan performed similar microcompression experiments using a nanoindenter at room temperature

* Corresponding author.
E-mail address: d.raabe@mpie.de (D. Raabe).

1359-6454/$30.00
doi:10.1016/j.actamat.2007.04.023

on Ni_3Al specimens [6]. Their columns, which were also produced via focused ion-beam milling, had a diameter of 2 μm.

By using finite element simulations with an isotropic constitutive law Zhang et al. [7] proposed some guidelines from a continuum mechanics point of view in terms of geometry and system set-up to design accurate microcompression tests. This is a sensible approach since finite element simulations are well suited to study details of the influence of the external boundary conditions and their possible changes during compression encountered in such tests. Points of particular interest in the paper were the effects of the strain-hardening behavior, the initial height and the Coulomb friction coefficient.

The motivation for the present study consists in merging some aspects of the different investigations quoted above into one simulation procedure. This means that we combine the advantages of an anisotropic crystallographic law for the constitutive description of the material in conjunction with a full consideration of crystallographic orientation effects and orientation evolution with proper boundary condition treatment via a crystal plasticity finite element simulation.

The aim of this approach is to address the compression deformation of cylindrical single crystal micropillars with respect to the role of the initial crystal orientation, evolution of deformation-induced orientation changes, sample geometry (diameter-to-length ratio), crystalline anisotropy and Coulomb friction on the course of such tests. Similar crystal plasticity finite element simulation approaches have been previously shown to be successful for investigating the relationship between mechanical boundary conditions and orientation effects at small scales, e.g. for the case of single crystal deformation [8], bicrystal deformation [9–11], oligocrystal deformation [12] and nanoindentation [13,14]. The results are used to investigate our hypothesis that even in the case of an homogeneous initial crystallographic orientation and homogeneous initial boundary conditions at the beginning of a compression test, gradual formation of orientation gradients can take place within an initially uniformly oriented specimen during loading.

2. Simulation procedure

2.1. Introduction

The finite element method is well suited to the treatment of complex boundary conditions in materials mechanics. Its concept is based on dividing (continuum) space into small domains with simple geometry which allows one to approximate the response to a given local constitutive behavior in such domains under the boundary conditions imposed jointly by external and internal constraints. Of importance in this paper is the use of a crystalline elastic and plastic anisotropic constitutive law [15].

In classical isotropic continuum mechanics, crystallographic rotations, and hence orientation effects, do not play a role since an antisymmetric portion associated with the dyadic nature of crystallographic dislocation slip (i.e. shear only along discrete directions on discrete planes) does not exist. This means that isotropic constitutive approaches to materials micromechanics are less useful in cases where the crystalline nature of matter plays an important role in terms of anisotropy and deformation-induced orientation changes including the formation of orientation gradients. An overview of the different approaches to the incorporation of crystalline anisotropy into finite element schemes is given in Refs. [15–20].

In this investigation the crystal plasticity finite element method is used to systematically study the intrinsic parameters (e.g. initial orientation and the evolution of deformation-induced orientation changes upon mechanical loading) and extrinsic effects (e.g. sample geometry and the contact conditions) involved in microcompression tests.

2.2. Constitutive model

2.2.1. Flow rule

In order to describe the flow kinematics the finite deformation defined by the deformation gradient, F, is multiplicatively decomposed into two contributions, namely the elastic and rotational part of the deformation gradient, F^*, and the plastic part of the deformation gradient, F_p [15]. The latter quantity describes an intermediate configuration accounting only for the deformation induced by the plastic slip in the lattice, i.e. $\det F_p = 1$. The elastic and rotational portion of the deformation gradient, F^*, captures both the stretch and the rotation of the lattice. The flow rule was used in the form:

$$\dot{F}_p = L_p F_p, \tag{1}$$

and the plastic velocity gradient, L_p, as:

$$L_p = \sum_\alpha \dot{\gamma}_\alpha (m_0^\alpha \otimes n_0^\alpha), \tag{2}$$

where m_0^α and n_0^α are the orthonormal vectors describing the slip direction and the slip plane normal of the slip system α in the reference configuration, respectively. $\dot{\gamma}_\alpha$ describes the shear rates on the slip systems α.

2.2.2. Hardening mechanism

The phenomenological hardening law is based on a crystal plasticity model which was suggested by Rice [15], Hutchinson [21] and Peirce et al. [16,17] for the face-centered cubic (fcc) lattice. The kinetic law on a slip system α follows:

$$\dot{\gamma}_\alpha = \dot{\gamma}_0 \left| \frac{\tau_\alpha}{s_\alpha} \right|^{1/m} \operatorname{sign}(\tau_\alpha), \tag{3}$$

where $\dot{\gamma}_\alpha$ is the shear rate on the slip system subjected to the resolved shear stress τ_α having a slip resistance of s_α. $\dot{\gamma}_0$ and m are material parameters and stand for the reference shear rate and for the rate sensitivity of slip, respectively. The influence of any slip system β on the hardening behavior of system α is given by:

$$\dot{s}_\alpha = \sum_\beta h_{\alpha\beta}|\dot{\gamma}_\beta|, \tag{4}$$

where $h_{\alpha\beta}$ is referred to as hardening matrix:

$$h_{\alpha\beta} = q_{\alpha\beta}\left[h_0\left(1-\frac{s_\beta}{s_s}\right)^\alpha\right], \tag{5}$$

which empirically captures the micromechanical interaction among different slip systems. In this formulation h_o, a, and s_s are slip hardening parameters, which are assumed to be identical for all fcc slip systems owing to the underlying characteristic dislocation reactions. The parameter $q_{\alpha\beta}$ is taken as 1.0 for coplanar slip systems α and β, and 1.4 otherwise, which renders the hardening model anisotropic.

2.2.3. Constitutive material parameters

The hardening parameters in Eqs. (3)–(5) for Cu were taken from Refs. [13,14], namely, $h_o = 180$ MPa, $a = 2.25$, $s_s = 148$ MPa and $m = 0.012$. The initial value of the slip resistance was chosen as 16 MPa and $\dot{\gamma}_o$ was taken to be 0.001 s^{-1}. The elastic constants were those for pure Cu, i.e. $C_{11} = 168$ GPa, $C_{12} = 121.4$ GPa, $C_{44} = 75.4$ GPa.

2.3. Finite element model and boundary conditions

The constitutive crystal plasticity model with the time integration procedure outlined above was implemented in the commercial FEM software MARC using the subroutine HYPELA2 [22], which allows user-defined material constitutive rules to be implemented.

The pillar-shaped compression samples for the simulations were modeled as perfect cylinders placed on a large substrate that has the same crystal orientation and hardening parameters as the pillar itself. Typical of all such pillar compression tests is the fact that the sample is connected with some curvature to the substrate bulk sample from which the pillar was cut. The radius where the pillar connects to the substrate amounts in all cases to a value of 30% of the pillar diameter (Fig. 1). The compression tool was treated as a rigid surface. The mesh consisted of 3376, 3952, 4528 elements (three-dimensional quadrilateral, eight integration points), respectively, and 3767, 4424, 5081 nodes, respectively, for specimens with different initial diameter-to-length ratios of 0.68, 0.4 and 0.29. The geometry is typical of some of the experimental work being conducted in this field.

In the formulation of the boundary condition, the nodes on the bottom of the substrate are not allowed to undergo displacements along the loading axis (*z*-axis) and the nodes among the bottom nodes on the lines which are parallel to *x*- and *y*-axis could not be displaced along the *y*- and *x*-axis, respectively. The version of the crystal plasticity finite element constitutive model used in this study does not include mechanical size effects and, therefore, takes account only of the relative variation in the diameter-to-length ratio but not of the fact that the original sample geometries reported in the literature are actually in the micrometer regime.

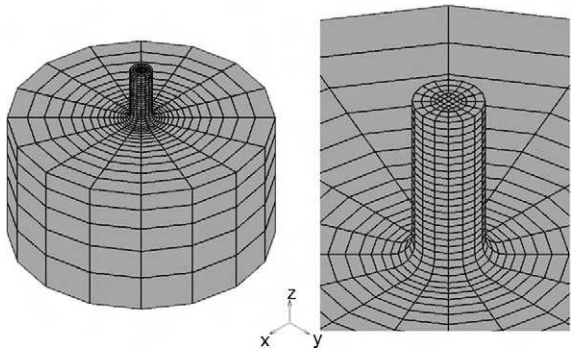

Fig. 1. Finite element mesh as used for the case of an initial diameter-to-length ratio of 0.4. Right-hand side: close-up view of the pillar. The chosen geometry is typical of some of the current experimental work being conducted in this field. As is usual for such tests, when the sample is prepared via cutting in a focused ion-beam (FIB) microscope, it is connected with some curvature to the substrate bulk sample from which the pillar was cut.

2.4. Modeling systematics

This study aims at a better understanding of the influence of the initial orientation, deformation-induced orientation changes including orientation gradient formation, sample geometry, anisotropy and friction in micropillar compression tests. In order to cover these aspects the simulations were divided in four groups:

- Group 1 (effect of sample height): different initial diameter-to-length ratios of 0.68, 0.4 and 0.29; same initial crystallographic orientation for all three tests ([1 1 1 2] compression axis); same Coulomb friction coefficient for all three tests ($\mu = 0.0$).
- Group 2 (effect of friction in case of unstable orientation): same initial diameter-to-length ratio of 0.4 for all three tests; same initial crystallographic orientation for all three tests ([1 1 1 2] compression axis); different Coulomb friction coefficients ($\mu = 0$, 0.05, 0.1).
- Group 3 (effect of friction in case of stable orientation): same initial diameter-to-length ratio of 0.4 for all three tests; same initial crystallographic orientation (exact [0 0 1] compression axis) for all three tests; different Coulomb friction coefficients ($\mu = 0.0$, 0.005, 0.05, 0.1).
- Group 4 (effect of friction in case of nearly stable orientation): same initial diameter-to-length ratio of 0.4 for all three tests; same initial crystallographic orientation (near-cubic orientation with a compression axis close to the [0 0 1] axis); different Coulomb friction coefficients ($\mu = 0.0$, 0.05, 0.1).

The reasoning behind this choice in the model parameters is the following. First, we want to study the influence of the stability of the initial orientation of the single crystal on the course of the compression tests. For this purpose we selected three different initial crystallographic orientations, namely a [1 1 1 2] compression axis, an exact [0 0 1] compression axis and a compression axis near the

[0 0 1] direction. The first orientation is known as a very unstable one upon compression [23]; we use it in order to probe a situation where the sample has a small crystallographic stability. An initial condition such as this might be expected to result in strong deformation-induced orientation changes, including orientation gradient formation, taking place during the simulated compression test. This situation is simulated in order to study the relationship between the crystallographic stability and the geometric stability of the pillar.

Opposing cases for crystallographic stability are examples with pronounced orientation changes upon loading vs. cases where the orientation is stable during loading (no deformation-induced orientation scatter upon straining). Opposing cases for geometric stability are examples with a strong shape change vs. situations with shape stability during testing.

The crystallographic stability criterion that we used for the selection of an unstable starting orientation uses the approach suggested in Ref. [23]. It is based on the divergence of the reorientation field for a given orientation under an imposed loading state. An orientation with a high reorientation divergence in orientation space means that tiny changes either in the external boundary conditions or in the internal state (e.g. some very small initial orientation spread) may entail drastic changes in the reorientation path upon plastic deformation. It must be underlined that a large value in the reorientation divergence (indicating high instability) is not due to a non-linear effect but simply due to a certain variety in the sets of potential slip systems with similar Schmid factors which, when activated, would entail a highly divergent rotation field in orientation space. In contrast to this unstable initial orientation, we have chosen as a second variant as a more stable orientation the cubic orientation with a [0 0 1] compression axis, the stability of which was investigated in detail in Refs. [23,24]. Owing to the high symmetry of this orientation under compressive load (eight slip systems have an identical Schmid factor), we have studied the same orientation again but with a slight orientation deviation of 0.1° from the exact [0 0 1] compression axis. This non-perfect [0 0 1] orientation is used as one of the starting orientations in order to mimic the effect of a slight asymmetry at the beginning of an experiment. We assume that an initial situation with a tiny deviation from the desired exact orientation relative to the compression tool is not too unrealistic owing to the complexity associated with the focused ion-beam (FIB) sample preparation and the subsequent compression technique. This selection, hence, alters the orientation spectrum from the most unstable to a rather stable orientation.

The other variations are obvious, i.e. the diameter-to-length ratio is relevant for modifying the buckling tendency of the pillar and the friction imposes loads which deviate from the pure compressive state, introducing a shear component in the deformation.

3. Simulation results and discussion

3.1. Group 1 (effect of sample height: different height, same initial unstable orientation, no friction)

The focus of this section is on the geometrical shape stability or, conversely, the buckling tendency of single crystalline pillar-shaped samples during the simulated compression ([1 1 1 2] compression axis). Fig. 2 shows the predicted evolution of the pillar shapes and of the deformation-induced orientation changes for the three cases (diameter-to-length ratios of 0.68, 0.4 and 0.29). A pronounced shape instability was observed for the slim pillars with diameter-to-length ratios of 0.4 and 0.29. The shape of the thick pillar with a diameter-to-length ratio of 0.68 remained stable during compression even up to large strains. The color coding in Fig. 2 shows the magnitude of the accumulated crystallographic plastic shear. It is revealed that in both cases where geometrical instability occurs (diameter-to-length ratios 0.4 and 0.29), the accumulated shear is localized close to the bottom of the pillar and close to the (friction-free) contact zone between the pillar and the compression tool. The strong shape changes observed for the slim pillars leads to a strong reduction of the contact zone between pillar and tool, and, hence, to corresponding strain localization and shear effects at the top of the pillars.

Although even the thickest pillar revealed a slight tendency for a shape instability, as indicated by the mesh distortion inside the compressed pillar, its geometrical constraints (large diameter) obviously exerted a stabilizing effect so that the overall pillar shape remained essentially cylindrical.

The model with an initial diameter-to-length ratio of 0.4 was chosen for the ensuing simulations below (groups 2–4) because it reveals some shape instability and at the same time relatively small localization effects. This is an advantage for studying crystallographic orientation changes and boundary condition effects in greater detail. Also, this value for the diameter-to-length ratio is close to some typical pillar shapes reported in the literature.

Although the shape instabilities observed in Fig. 2 (middle and left columns) appear at first sight like a classical elastic–plastic buckling effect, they may to some extend be attributed to the strong influence of the crystalline anisotropy created by the single crystalline material constitutive law. Classical analytical models predict that plastic buckling may be expected to occur for pillars which are at least about a factor of 20 longer than in the current case (assuming the same diameter), i.e. classical isotropic solutions to predicting buckling of such pillars do not apply. Also, the shape instability observed does not resemble a classical buckling phenomenon but rather a unidirectional bulk shear process of the entire specimen with two main localization zones. The first zone is close to the bottom of the pillar and the second one is located in the contact zone to the tool. The observation that classical buckling

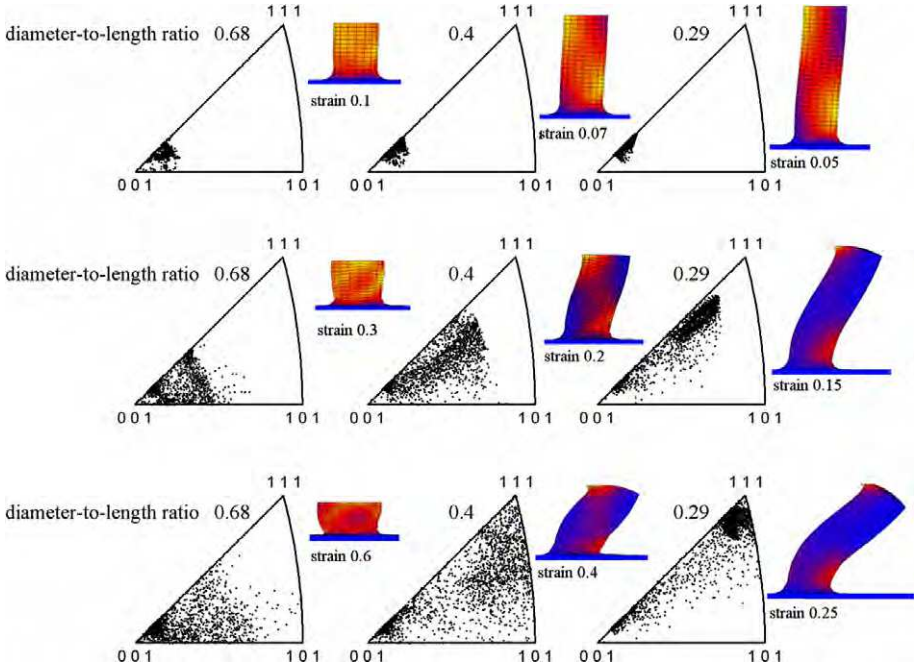

Fig. 2. Crystallographic orientation changes and shapes of three pillars with different initial dimensions (diameter-to-length ratios: 0.68 (left), 0.4 (middle), 0.29 (right)) after different displacements (color coding accumulated plastic shear from blue (low) to yellow (large)). Starting single crystal orientation: [1 1 12] compression axis (unstable). The strain is given as an engineering thickness reduction.

theory does not apply for single crystal compression may be attributed to the discreteness of the plastic slip in the case of the present crystal plasticity finite element simulation method.

The analysis of the active slip systems reveals that during the early stage of plastic deformation the activation of the slip systems is at first still homogeneously distributed throughout the volume of the compressed samples. In the slim pillars this early stage was followed by pronounced shear localization phenomena at the region close to the bottom of the pillars and in the contact region, which becomes smaller during the simulated test owing to the strong shape change and bending of the slim pillars. As mentioned above, this effect seems to favor a bulk shear deformation of the entire shape.

The difference in the orientation evolution between the three different types of originally single crystalline samples is quite remarkable. The shortest and geometrically most stable (in terms of shape) sample (largest diameter-to-length ratio of 0.68, left-hand side in Fig. 2) reveals a strong spread of the initial orientation after deformation into an orientation distribution which is characterized by rotations towards the [1 1 1] direction and particularly towards the [1 0 1] direction. The [1 0 1] compression axis would be the most stable final crystal orientation for the case of conventional frictionless uniaxial compression of fcc single crystals according to a simple Schmid calculation. Although the other orientations with high symmetry are also mathematically stable, already small deviations from the exact orientation would entail irreversible orientation changes. In contrast, small changes away from an exact [1 0 1] compression axis would always entail a back rotation into that orientation.

The other two compression samples (diameter-to-length ratio of 0.4 and 0.29) are geometrically less stable and, hence, undergo a pronounced shape distortion entailing complete sample inclination. This phenomenon strongly affects the resulting orientation spread observed in the two simulation series. In both cases the orientation distribution evolves towards the [1 1 1] direction. This effect is particularly pronounced in the case of the geometrically most unstable sample (diameter-to-length ratio 0.29), where a very strong [1 1 1] orientation distribution is formed after 25% engineering thickness reduction.

This strong effect can be obviously explained by the pronounced inclination of the shape during the compression. Since the orientation changes plotted in the inverse pole figures are calculated by using the initial sample coordinates as a reference coordinate system, the strong evolution of the initially homogeneous single orientation into a complex orientation distribution towards the [1 1 1] direction is in part not only of a crystallographic nature but contains contributions from the inclination of the specimen. In other words the local sample reference coordinates in the distorted specimen have changed more dramatically in this case than the actual crystallographic orientation was rotated by homogeneous slip. This means that all orientation points shown in the inverse pole figure are geometrically misoriented in the order of the magnitude of the inclination angle between the (new inclined) sample axis and the bottom normal. Fig. 3 explains these two different effects. The plastic spin which is solely due to

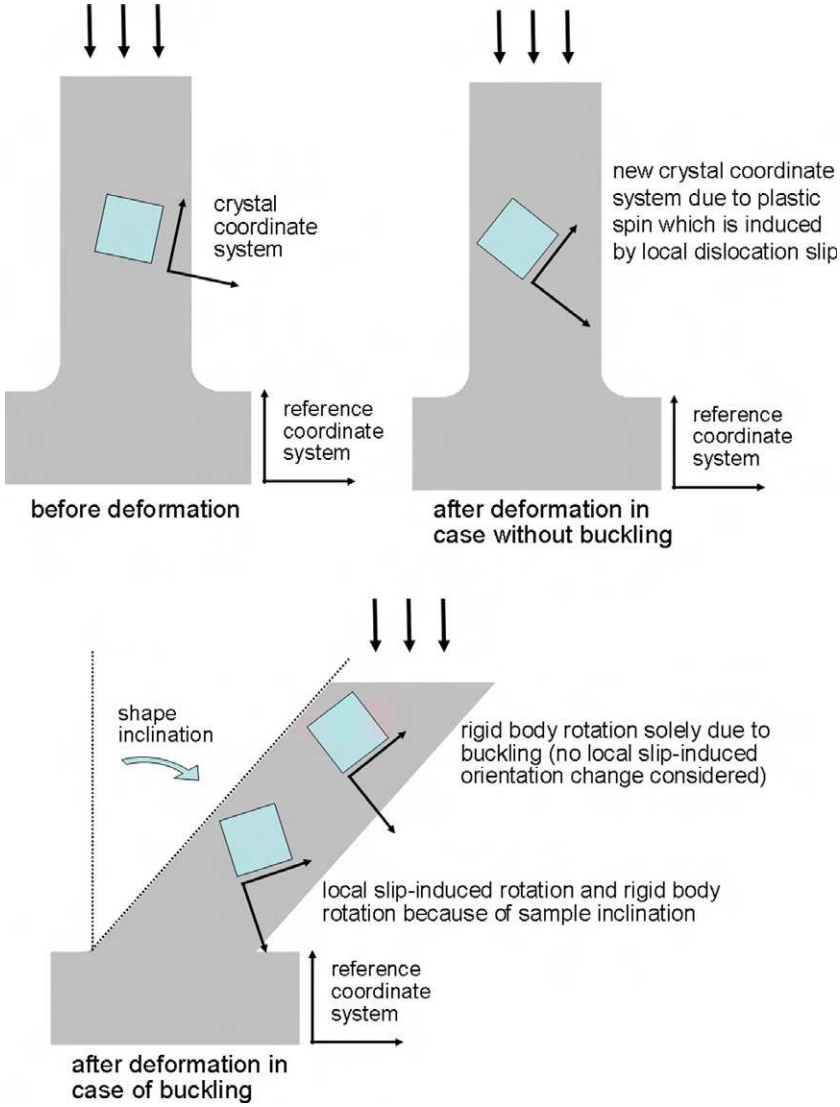

Fig. 3. Schematic figure of the influence of the change in the coordinate system upon compression and its effect on a geometrical component of the orientation distribution presentation when referred to the original reference coordinate system.

dislocation-induced crystallographic orientation changes results from the antisymmetric portion of the displacement gradient tensor that is created by (homogeneous) dislocation slip. Fig. 3 shows that further rotations can be created when inclination (buckling) of the reference system occurs. This effect is due to rigid body rotations upon changes in the macroscopic sample geometry. Of course, this buckling effect is also due to dislocation slip, but it is highly localized in one particular zone where the curvature is largest. This effect entails apparent additional orientation changes, which have to be distinguished from the crystallographic portion of the plastic spin.

Besides these basic explanations on the possible origin of deformation-induced orientation changes it must also be underlined in general that the simulations presented in this work do not account for the strong localization of dislocation slip as observed in the experiments [1–5] but rather anticipate slip homogeneity as expressed in Section 2.2. This difference between the real and the simulated collective dislocation flow might also affect the predicted orientation changes. Since the skew-symmetric portion of the displacement gradient tensor (plastic spin) is generally independent of the details of the dislocation distribution we assume that possible differences between experimentally observed and simulated orientation changes might be due to differences in the local hardening behavior rather than to basic differences in the kinematics.

3.2. Group 2 (effect of friction in the case of an unstable orientation: all pillars with same initial thickness and same initial unstable orientation, different friction coefficients)

The group 2 results on the change in the stress distribution together with the pillar shapes and the crystallographic

orientation distributions are shown in Fig. 4a and b for different strains. Fig. 4a uses individual color spreads for each image to reveal patterning phenomena. The deformation-induced orientation changes in the sample which was deformed with a zero friction coefficient (left columns in Fig. 4a and b) reveal a very strong tendency for reorientation with particular preference towards the evolution of a crystallographic [1 1 1] orientation distribution inside the initially uniform crystal (Fig. 4b).

The other two specimens which were deformed under non-zero friction conditions reveal slower orientation changes. In these two samples the initial orientation evolves towards the [1 1 1] and the [1 0 1] axis (middle and right columns of Fig. 4a and b). Also, the overall spread in the deformation-induced orientation distribution is in both cases with non-zero friction much smaller than in the case with zero friction. The latter simulation (zero friction, left column) reveals a large deformation-induced

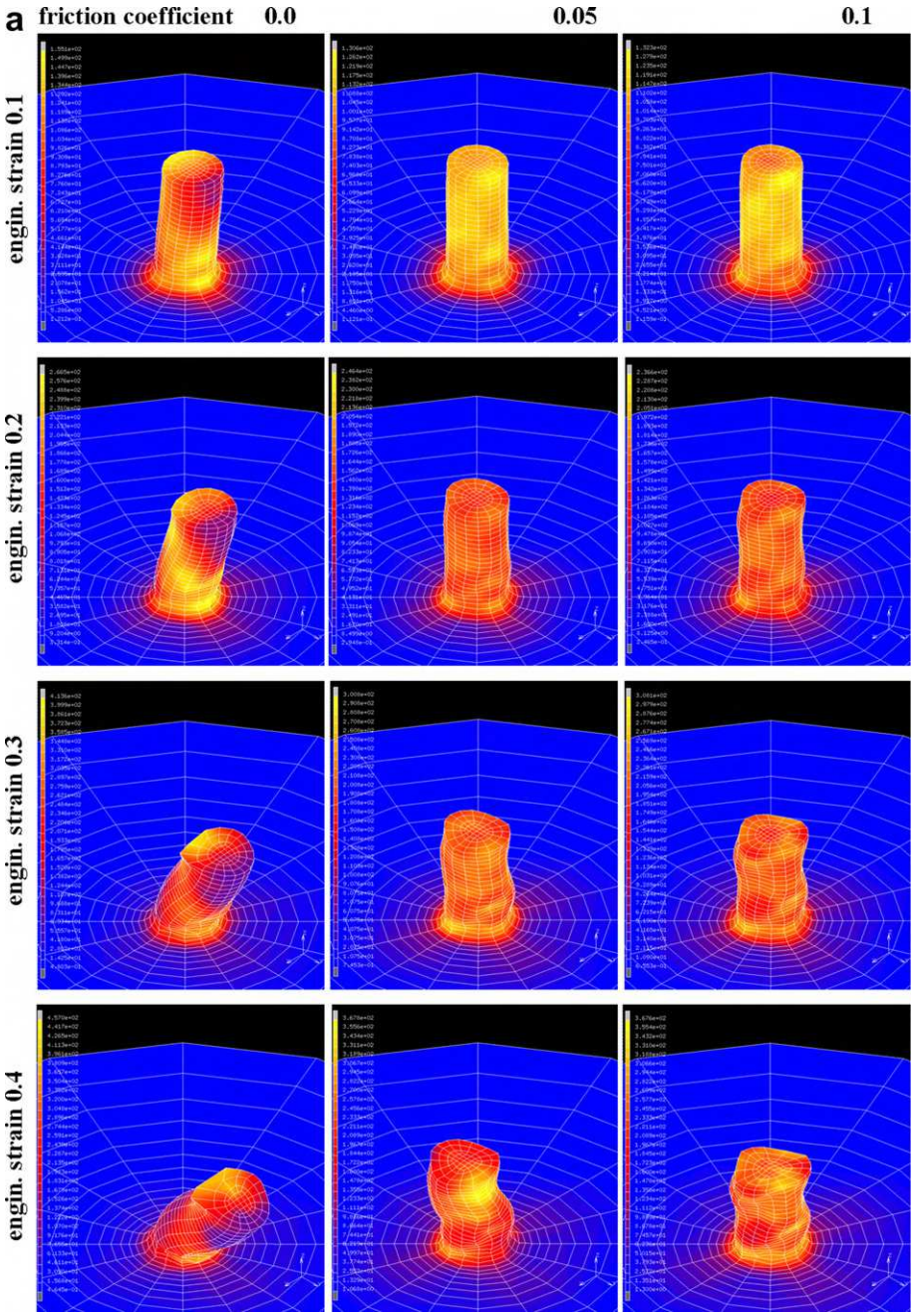

Fig. 4. Crystallographic orientation distribution and shapes of pillars with an identical initial diameter-to-length ratio of 0.4, deformed assuming different Coulomb friction coefficients (0.0 (left column), 0.05 (middle column), 0.1 (right column)). Starting single crystal orientation: [1 1 1 2] compression axis, unstable against compression. (a) Presentation of the pillar shapes. Color coding: equivalent von Mises stress from blue (low) to yellow (large). Individually chosen color spread for each image to reveal patterning phenomena. (b) Orientation scatter in inverse pole figures. (c) Engineering stress vs. engineering strain curves for the three cases with different friction coefficients (σ = stress, $d\sigma/d\varepsilon$ = hardening).

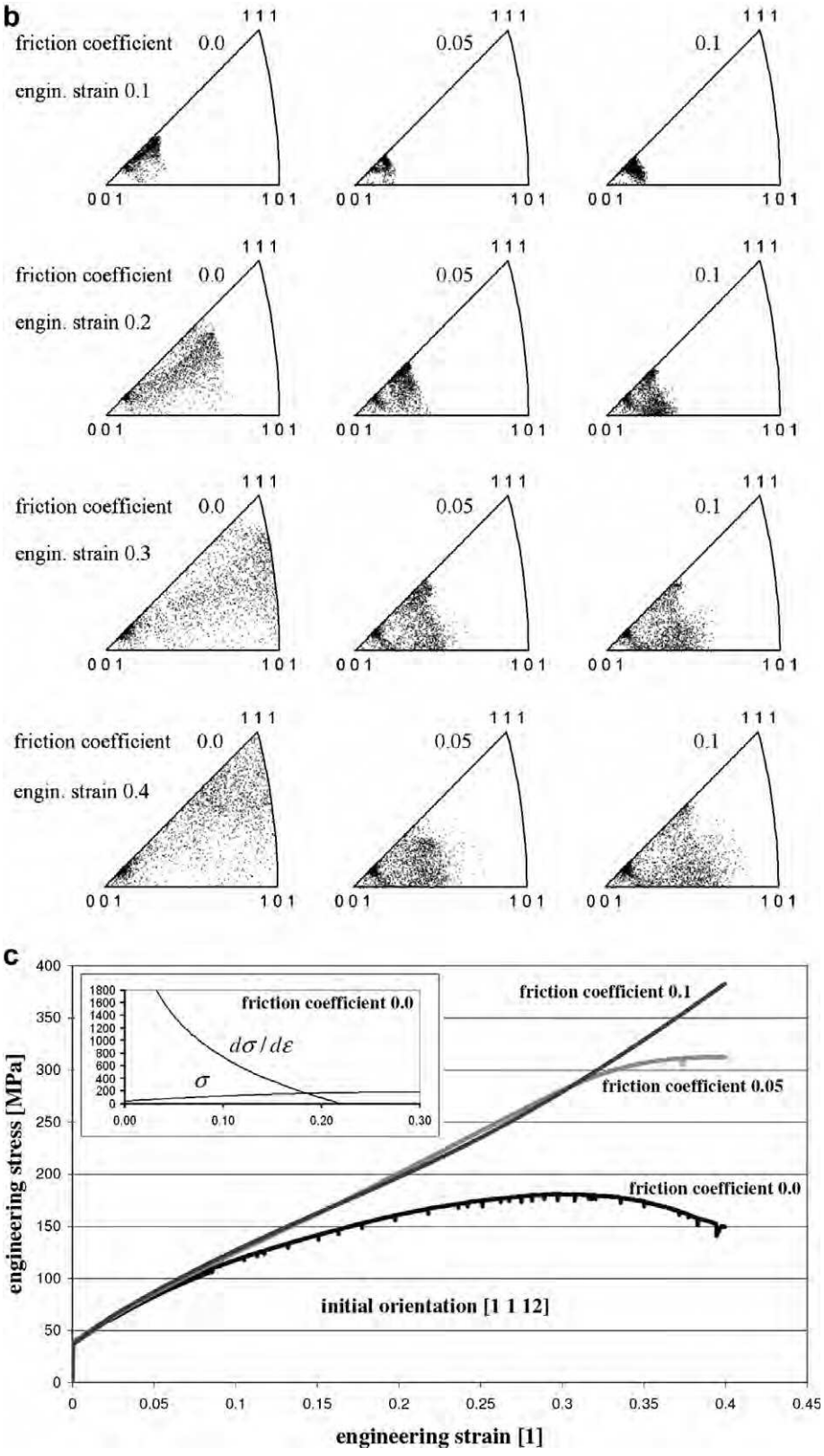

Fig. 4 (*continued*)

orientation spread covering nearly the entire standard triangle. The results clearly confirm that the chosen initial crystal orientation is in all three cases very unstable against compression. This observation matches earlier results on the kinematical origin of the stability of this orientation [23].

The shape changes of the pillars also reveal clear differences among the three samples (Fig. 4a). The sample that was deformed under zero-friction conditions shows a very strong buckling effect, while the two specimens that were deformed with non-zero friction conditions reveal a more stable evolution of the shape, i.e. less buckling. This applies in particular to the case with the largest friction coefficient of 0.1 (right column in Fig. 4a).

This observation is also reflected by the corresponding flow curves. For the case with zero friction, the stress–strain curve for the sample with initial [1 1 1 2] orientation reveals that the simulated test becomes unstable at an early stage of deformation (Fig. 4c). This observation matches the shape change presented in Fig. 4a. The stability of the flow curve is analyzed in terms of the Considère criterion, i.e. in terms of the point of intersection between the stress–strain curve and its derivative (upper left diagram in Fig. 4c). The point of intersection between the two curves occurs at an engineering strain of 0.185. The two stress–strain curves for non-zero friction conditions (friction coefficients of 0.05 and 0.1) are much more stable and do not experience geometrical softening. Such behavior is typical of conventional bulk compression tests, which as a rule do not undergo geometrical softening but instead shape stabilization in cases when the diameter-to-length ratio is much larger than the critical ratio at which buckling occurs. The unstable stress–strain curve for zero friction reflects the shape instability of the zero-friction specimen under load. It must be considered in that context that shape instability may occur for anisotropic (single crystalline) constitutive elastic–plastic behavior at much lower strains than for isotropic behavior, i.e. conventional isotropic buckling theory does not apply. The two samples with friction coefficients of 0.05 and 0.1 reveal practically identical hardening behavior. At large strains above 0.35, the sample with a friction

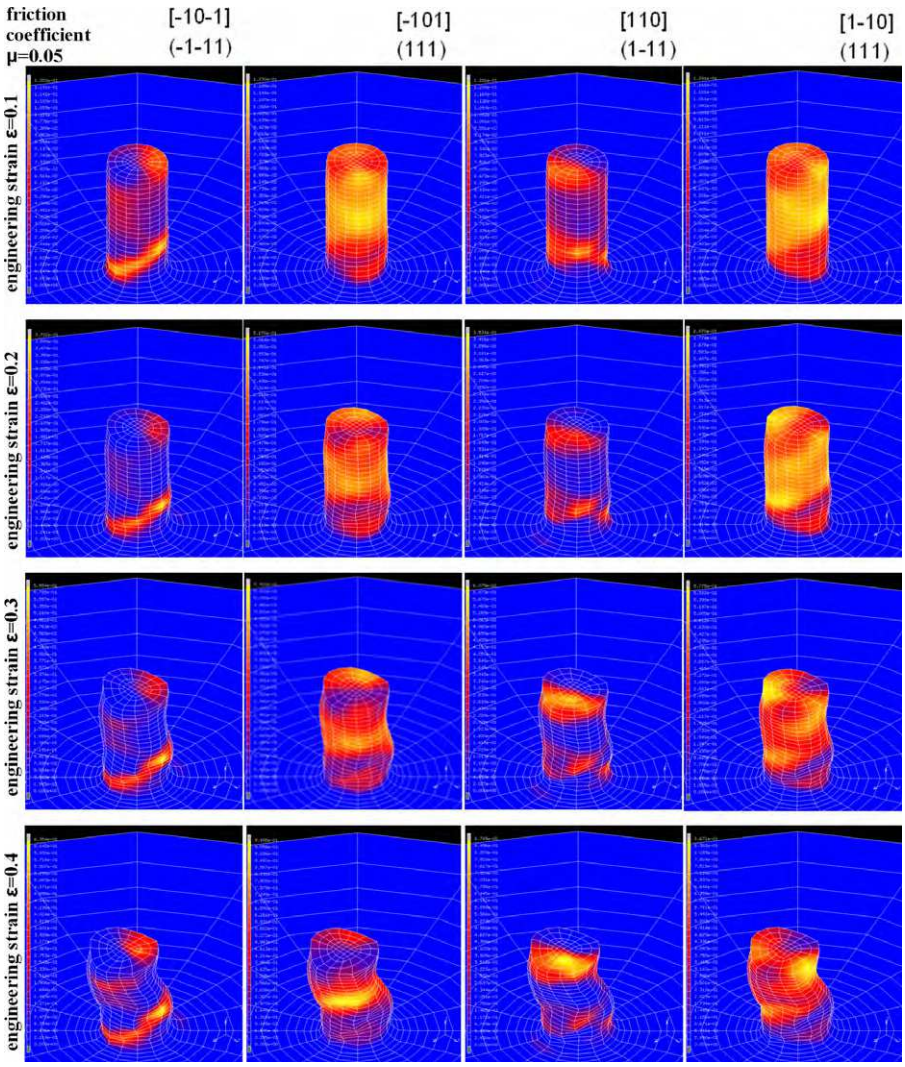

Fig. 5. Shear distribution on the four most active slip systems for the pillar with an initial diameter-to-length ratio of 0.4; Coulomb friction coefficient 0.05. (Color coding: accumulated crystallographic shear on the slip systems indicated above the images from blue (low) to yellow (large)). Initial single crystal orientation: [1 1 1 2] compression axis, unstable against compression. Individually chosen color spread for each image to reveal the shear patterning.

coefficient of 0.05 shows some softening, which can be attributed to shape instability. The predicted hardening is in all cases much larger than observed in microcompression experiments [1–5]. The reason for this discrepancy is that the current viscoplastic hardening constitutive model which is used in conjunction with the crystal plasticity formulation (see Section 2) does not account for any size or dislocation starvation effect such as discussed in the context of corresponding experiments.

Figs. 5 and 6 show the shear distribution on the four most active slip systems for the pillar with an initial diameter-to-length ratio of 0.4 at a Coulomb friction coefficient of 0.05 (Fig. 5) and 0.1 (Fig. 6), respectively (sample with [1 1 1 2] compression axis, see Fig. 4a and b). The color coding refers to the magnitude of accumulated crystallographic shear on the slip systems. Yellow indicates the largest and blue the smallest amount of crystallographic shear. Note that the color spread has been individually chosen for each image to better reveal the shear patterning at all strains.

In both cases (friction coefficients of 0.05 and 0.1) the shear on the slip system $[\bar{1}\,0\,\bar{1}](\bar{1}\,\bar{1}\,1)$ is highly localized in an oblique shear band which crosses the pillar close to the bottom (left column in both figures). This zone of concentrated slip occurs already at an early stage of the simulated compression test. The shear on the slip system $[\bar{1}\,0\,1](1\,1\,1)$ is more equally distributed in the pillar (second column in both figures). At larger strains it is particularly concentrated in the zone where buckling occurs first. The shear distribution on the slip system $[1\,1\,0](1\,\bar{1}\,1)$ reveals in both cases (friction coefficients of 0.05 and 0.1) a concentration of crystallographic shear at the top of the pillar where tool contact occurs, and at the bottom close to the transition zone between the pillar and the bulk material below it (third column in both figures). The shear on the slip system $[1\,\bar{1}\,0](1\,1\,1)$ is more equally distributed through-

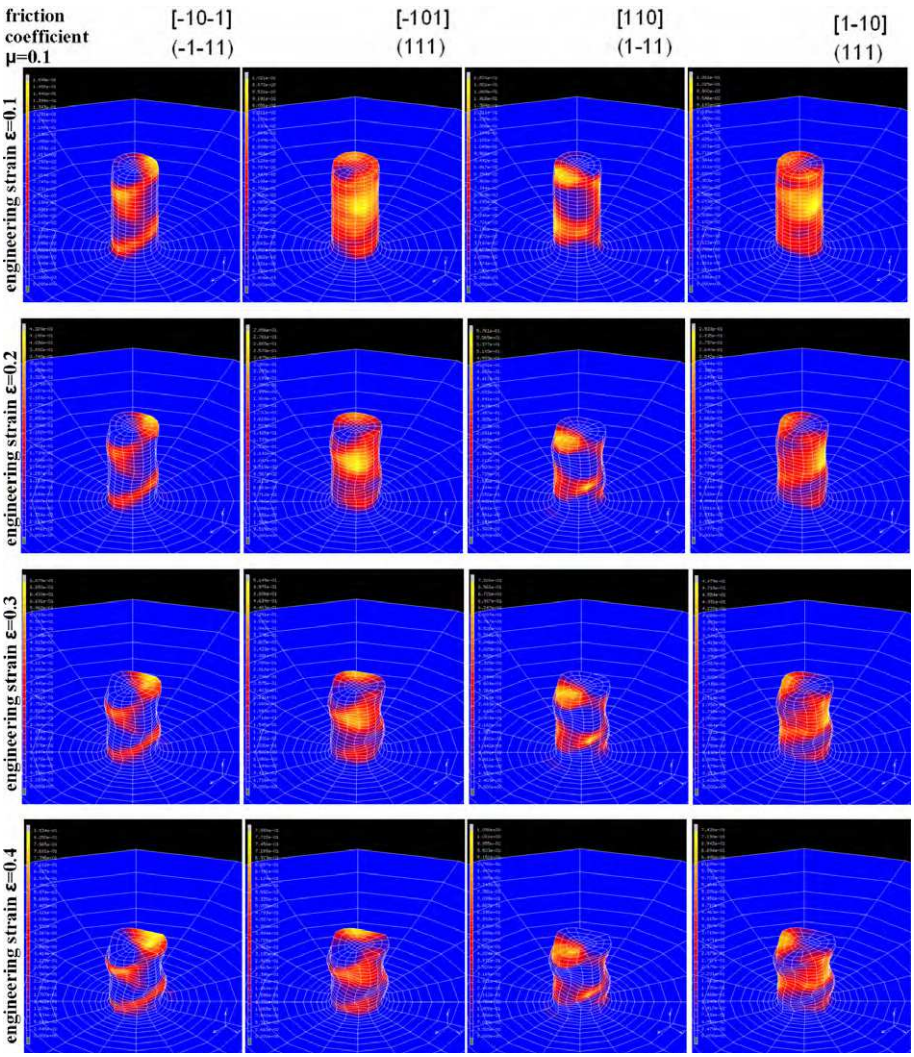

Fig. 6. Shear distribution on the four most active slip systems for the pillar with an initial diameter-to-length ratio of 0.4; Coulomb friction coefficient 0.1. (Color coding: accumulated crystallographic shear on the slip systems indicated above the images from blue (low) to yellow (large)). Initial single crystal orientation: [1 1 1 2] compression axis, unstable against compression. Individually chosen color spread for each image to reveal the shear patterning.

out the pillar with dominance in those zones where buckling occurs.

The strong localization of slip on the systems $[\bar{1}0\bar{1}](\bar{1}\bar{1}1)$ and $[1\,1\,0](1\,\bar{1}\,1)$ in the form of oblique shear zones coincides with the occurrence of strong shape instabilities in the pillars. The fact that the shape changes observed in the present examples cannot be interpreted in terms of classical analytical Eulerian solutions or plastic buckling theory suggests that it is the crystalline anisotropy which promotes early shape instability owing to its directional discreteness of the shear distribution. This effect obviously cannot be captured by isotropic buckling theory.

Another important observation is that the simulation with the higher friction coefficient (0.1; see Fig. 6) does not reveal a more homogeneous distribution of the crystallographic shear than the simulation with the smaller friction coefficient (0.05; see Fig. 5).

3.3. Group 3 (effect of friction in the case of a stable orientation: all pillars with same initial thickness and same initial stable orientation, different friction coefficients)

The exact cubic orientation with a [0 0 1] compression axis is known to be kinematically relatively stable for fcc single crystals under compressive loads as was investigated in detail in Refs. [23,24]. Owing to the high symmetry of the exact cubic orientation under compression (eight slip systems with an identical Schmid factor), we have selected in group 3 a set of friction coefficients modified from the other examples since it has been observed previously that minor changes in friction can have a substantial influence on the stability of this orientation when subjected to a compressive load.

Under compressive loads the cubic-oriented single crystals ([0 0 1] compression axis) reveal pronounced differences

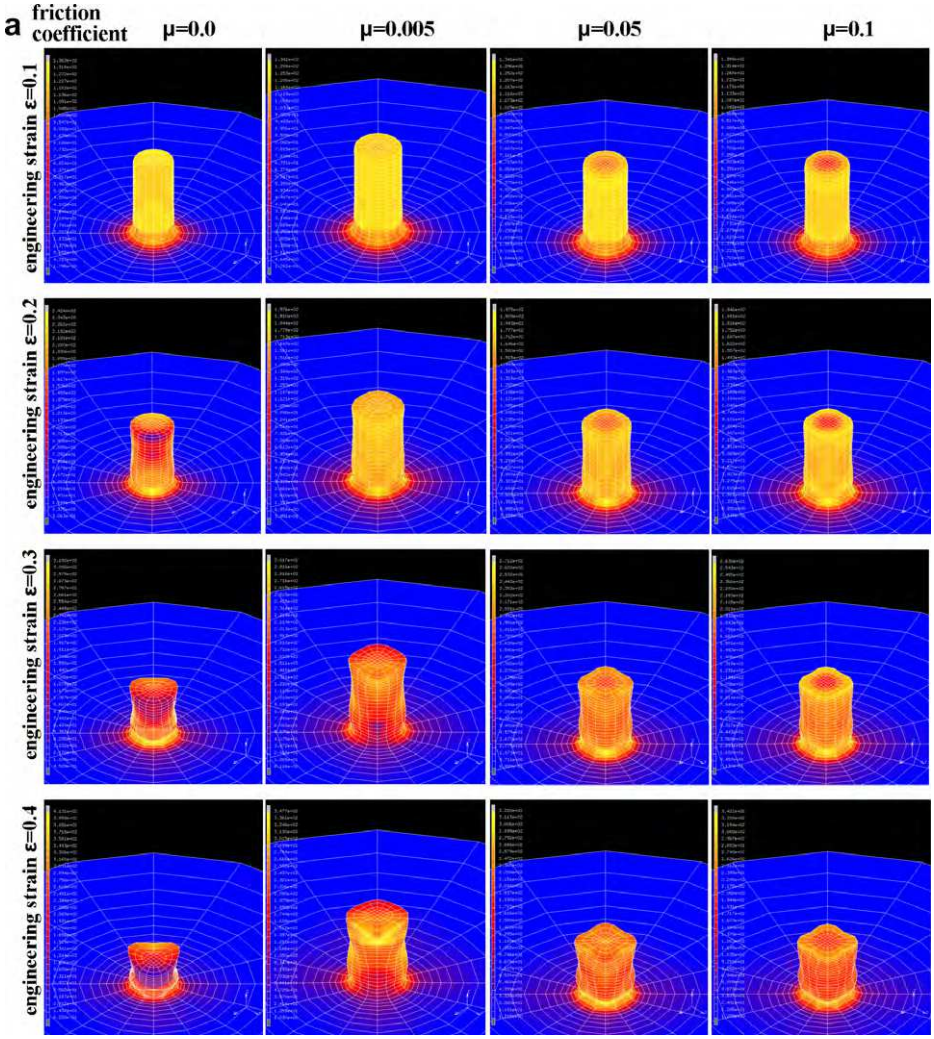

Fig. 7. Crystallographic orientation distribution and shapes of pillars with identical initial diameter-to-length ratio of 0.4 which were deformed assuming different Coulomb friction coefficients (0.0 (left column), 0.005 (left middle column), 0.05 (right middle column), 0.1 (right column)). Initial single crystal orientation: cubic orientation, [0 0 1] compression axis. (a) Presentation of the pillar shapes. Color coding: equivalent von Mises stress from blue (low) to yellow (large). Individually chosen color spread for each image to reveal patterning phenomena. (b) Orientation scatter in inverse pole figures. (c) Engineering stress vs. engineering strain curves for the four cases with different friction coefficient (σ = stress, $d\sigma/d\varepsilon$ = hardening).

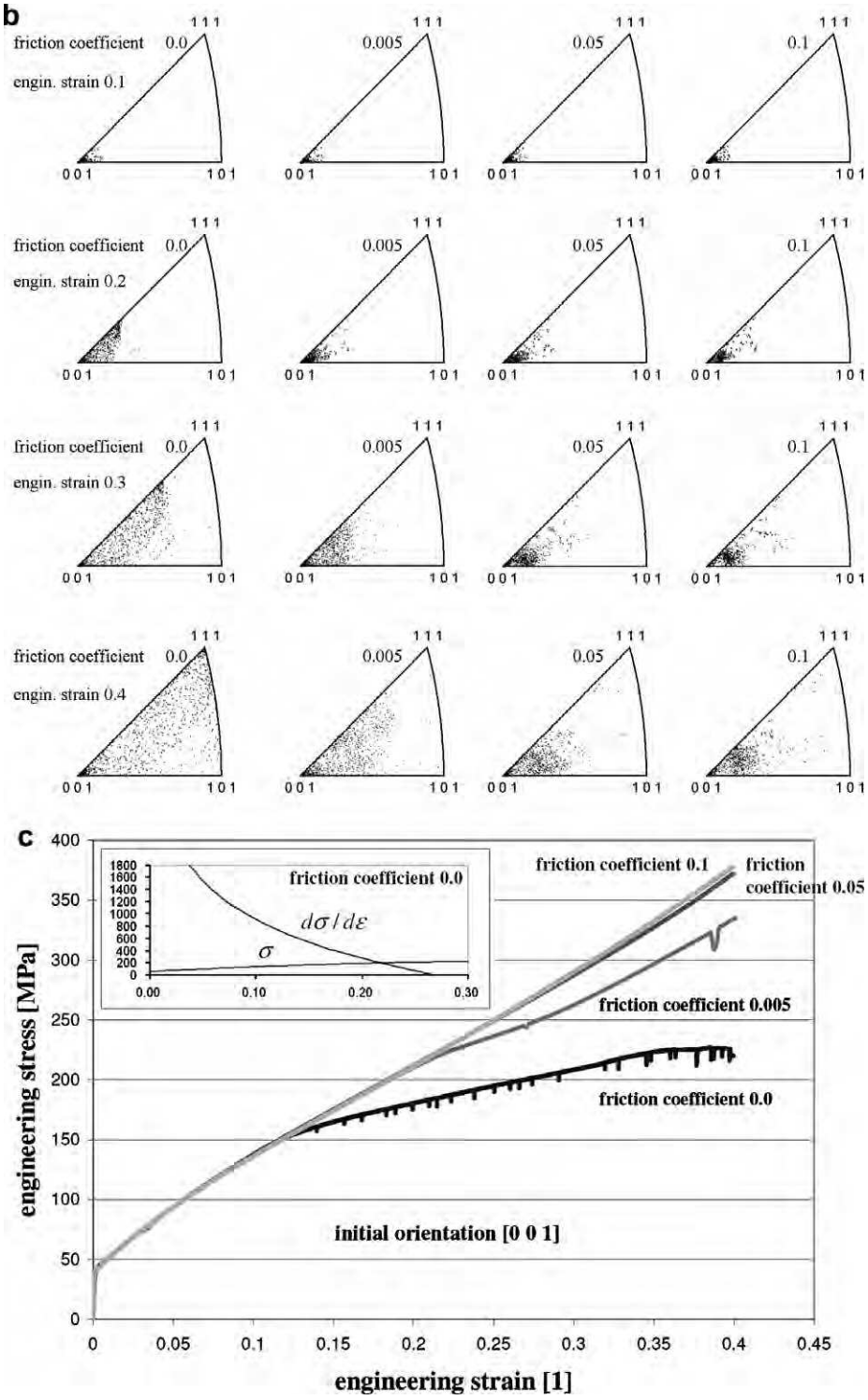

Fig. 7 (*continued*)

in shape change and orientation evolution as a function of the friction coefficient (Fig. 7a–c and Fig. 8). Slight differences in the apparent pillar height in Fig. 7a are due to perspective and differences in buckling. One should note that the color spread has been individually chosen for each image to better reveal the individual stress patterns for the subsequent loading stages. Fig. 7b shows the deformation-induced orientation scatter in terms of inverse pole figures. The (homogeneous) shape changes of the pillars are similar for the three cases with non-zero friction coefficients (0.005, 0.05, 0.1) (Fig. 7a). Similar to the observations for the preceding case with a less stable starting orientation (Fig. 4a and b), the [0 0 1] oriented samples evolve in all cases a deformation-induced orientation evolution includ-

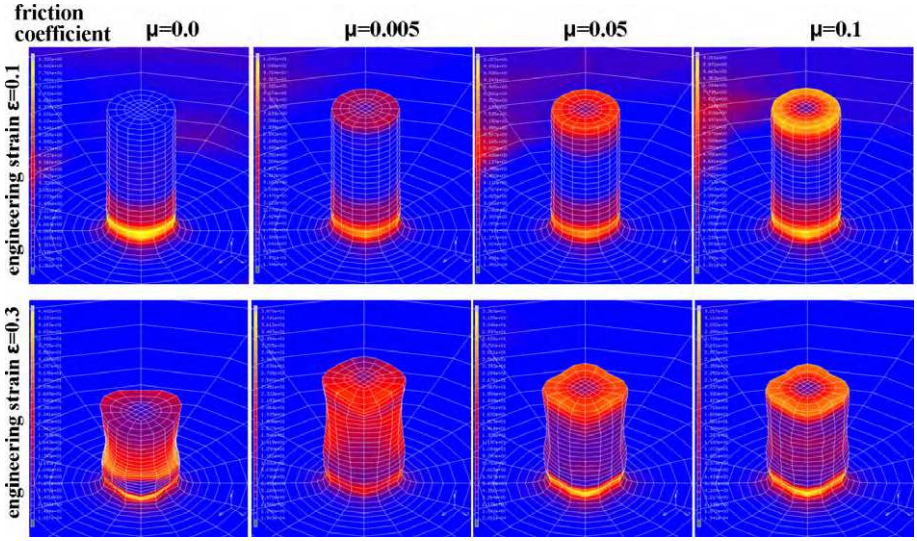

Fig. 8. Crystallographic orientation distribution within pillars with respect to the initial orientation for two deformation stages. Pillars with identical initial diameter-to-length ratio of 0.4 which were deformed assuming different Coulomb coefficients (0.0 (left column), 0.005 (left middle column), 0.05 (right middle column), 0.1 (right column)). Starting single crystal orientation: cubic orientation, [0 0 1] compression axis. Color coding: misorientation (angle only, axis not indicated) with respect to the original cubic orientation from blue (low orientation deviation to the original orientation) to yellow (large orientation deviation to the original orientation). Individually chosen color spread for each image to reveal patterning phenomena.

ing in part a large orientation spread (Fig. 7b). In the case of the zero friction compression test, the gradual formation of a very strong orientation spreading out from an originally single crystal orientation is by far the strongest owing to the distorted and inclined shape of the sample after straining (see explanation in Fig. 3). As pointed out above, this strong orientation change (see left column in Fig. 7a) is caused in part by the change in the reference shape and not only by crystallographic reorientation (Figs. 3 and 8).

In contrast to the cases discussed above with a less stable orientation, the present results on the [0 0 1] compression axis suggest that crystallographically symmetric orientations reveal a slightly better shape stability during compression than less symmetric orientations (see results in preceding section).

Although the shapes of the [0 0 1]-oriented pillars reveal a strong four-fold anisotropy in the cross section after straining under non-zero friction (e.g. bottom row in Fig. 8), the specimens do not undergo any buckling during compression. Buckling only occurred for the case with zero friction (Fig. 7a and Fig. 9). This observation indicates the important role played by crystallographic symmetry on the

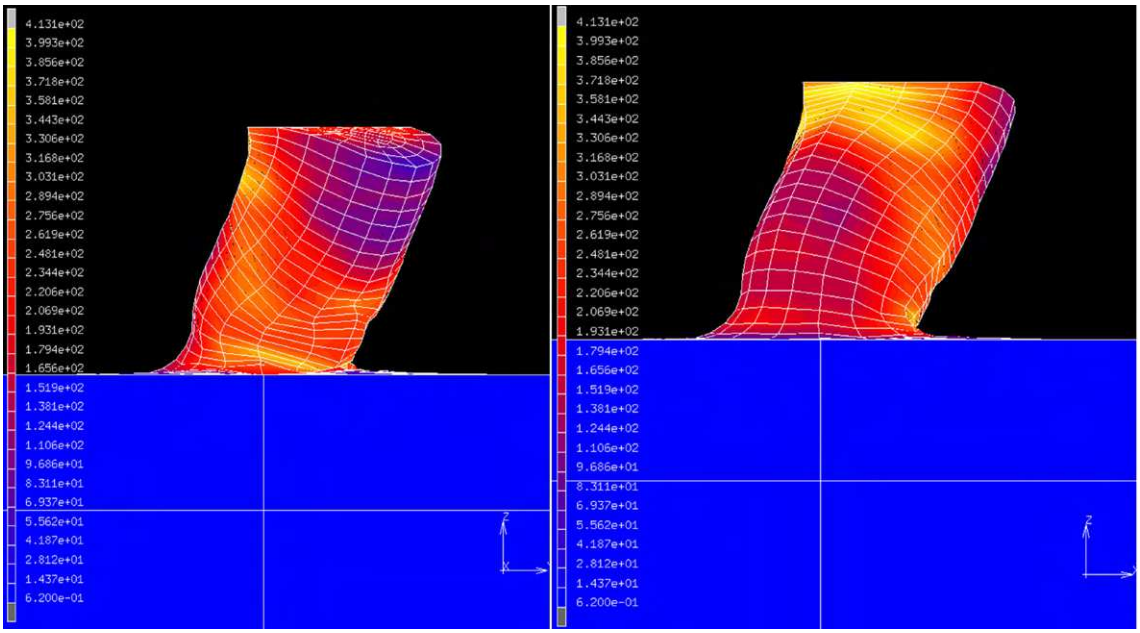

Fig. 9. Front and back view of the shape change of the pillar with an initial [0 0 1] axis compressed at zero friction to 40% engineering thickness reduction. Pillar with initial diameter-to-length ratio of 0.4. Color coding: von Mises stress from blue (low) to yellow (large).

one hand, and of friction on the other, in successful, buckling-free compression experiments. The observation of the stabilizing influence of friction is essential since in real experiments it is very difficult to prepare a sample with an exact desired orientation. An important point that deserves attention in that context is the possible influence of numerical aspects on the predicted buckling behavior. For instance, for the zero-friction boundary conditions, the high symmetry of the [0 0 1] compression load case and the absence of any shear forces at the beginning of the simulation would suggest higher shape stability than observed in the present case (Fig. 9). We therefore attribute the early shape instability observed even for highly symmetric situations also to some extent to numerical aspects

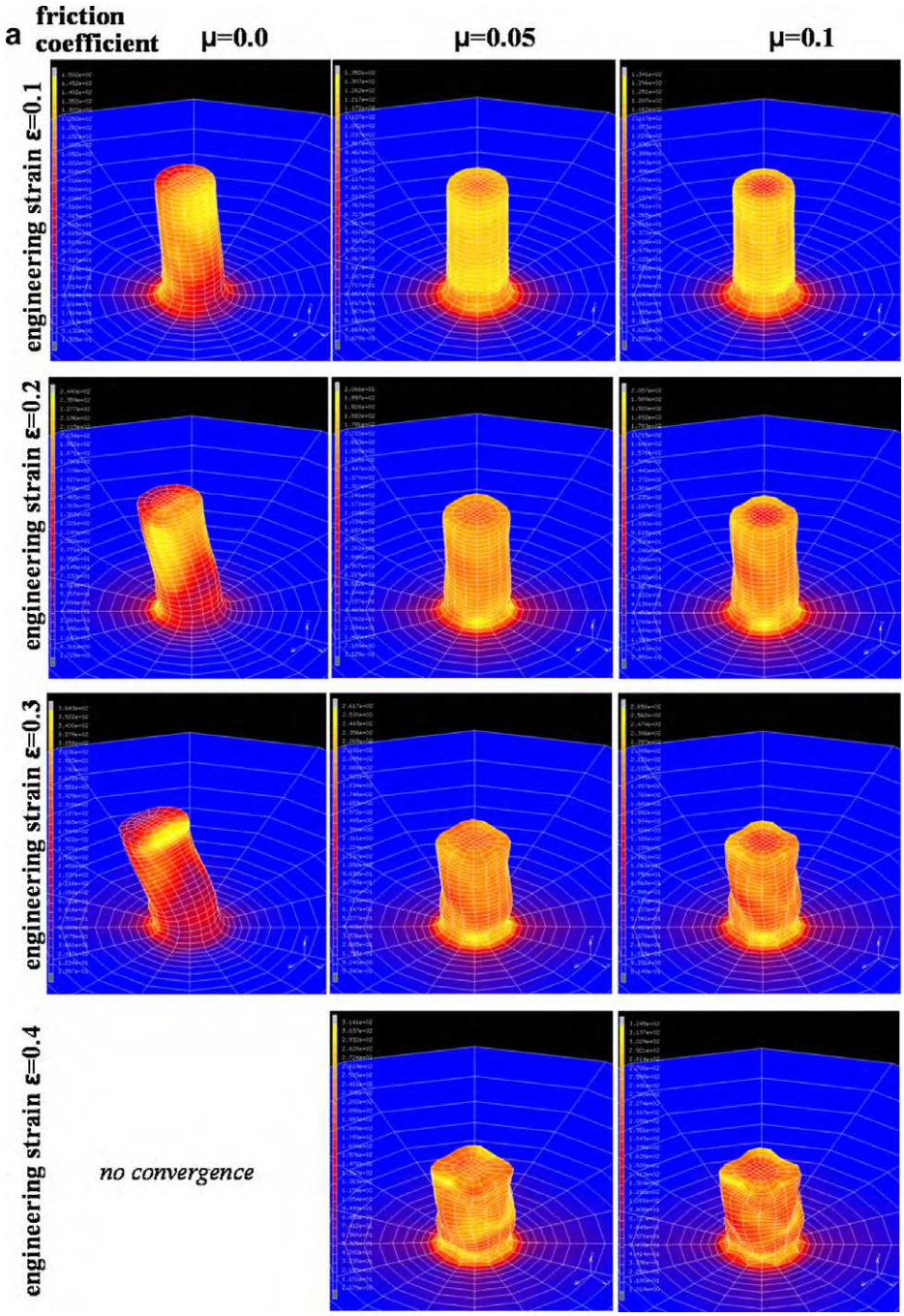

Fig. 10. Crystallographic orientation distribution and shapes of pillars with identical initial diameter-to-length ratio of 0.4 which were deformed assuming different Coulomb friction coefficients (0.0 (left column), 0.05 (middle column), 0.1 (right column)). Initial single crystal orientation: near [0 0 1] compression axis (0.1° initial deviation). (a) Presentation of the pillar shapes. Color coding: equivalent von Mises stress from blue (low) to yellow (large). Individually chosen color spread for each image to reveal patterning phenomena. (b) Orientation scatter in inverse pole figures. (c) Engineering stress vs. engineering strain curves for the three cases with different friction coefficient (σ = stress, $d\sigma/d\varepsilon$ = hardening).

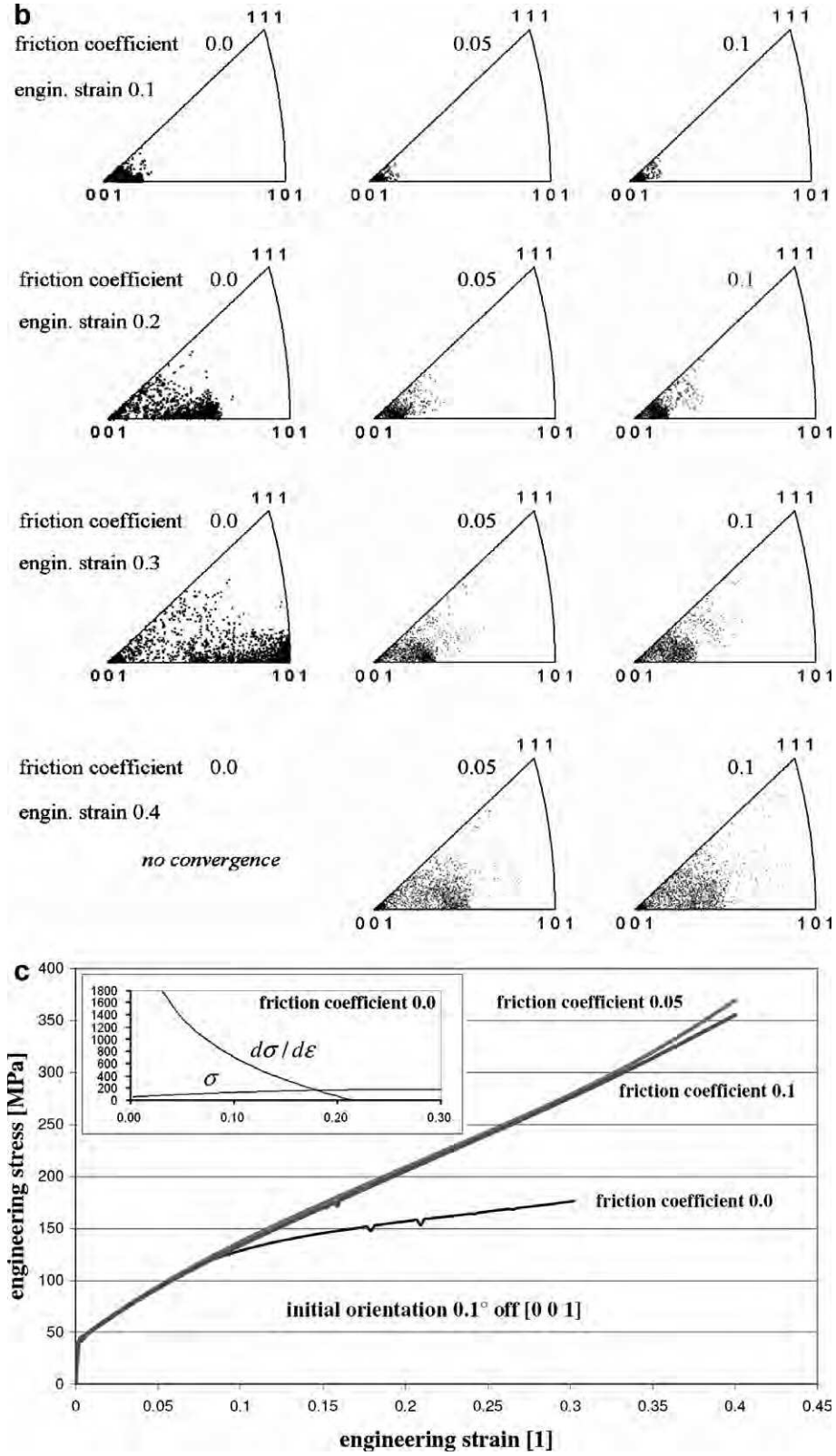

Fig. 10 (*continued*)

associated with the integration of the crystal plasticity constitutive law. The simulation results observed for slightly off-cubic situations, which are no longer perfectly symmetric, indeed indicate that even minor deviations (be they of a crystallographic or of a numerical nature) induce strong strain localization and shape change effects.

These observations on the shape changes for the different simulated single crystal compression tests correspond to the flow curves (Fig. 7c). For the relatively unstable case with zero friction the stress–strain curve shows that the test becomes unstable at an early stage of deformation. This observation matches the observed shape change (Fig. 9). The Considère analysis (point of intersection between the stress–strain curve and its derivative: upper left diagram in Fig. 7c) shows that instability starts at an engineering strain of 0.22. This value is small compared to the excellent stability of the simulated tests conducted with non-zero friction conditions, but it is high compared to the small value of 0.185 observed for the crystallographically less stable sample [1 1 12] (Fig. 4c). This means that the geometrical stability of single crystal compression tests can be improved by choosing stable orientations. The three stress–strain curves for non-zero friction conditions (friction coefficients of 0.005, 0.05 and 0.1) are much more stable and do not experience substantial geometrical softening.

Another important characteristic of the simulations with [0 0 1] compression axis as the starting single crystal orientation is the pronounced localization of the misorientation in a narrow band at the bottom of the compression samples close to the transition into the bulk material (Fig. 8). This observation holds for samples with all friction conditions. Those samples which were deformed with a non-zero friction coefficient also show a thin layer with strong misorientations to the tool at the contact area.

While the localization at the bottom of the sample can be attributed to the change in the boundary conditions owing to the curved transition into the bulk material, the misorientation localization at the contact zone for samples deformed under friction is due to the shear created in this thin contact zone. Both aspects deserve close attention for the design of optimal compression tests since strong localization effects (misorientation or strain or both) are obviously not desired for such tests.

3.4. Group 4 (effect of friction in the case of a nearly stable orientation: all pillars with same initial thickness and same nearly stable initial orientation, different friction coefficients)

The last example describes a nearly stable single crystal. The initial orientation before deformation deviates by only 0.1° from the exact [0 0 1] compression axis (Fig. 10a–c). Although this deviation appears as a small orientation difference, we think that its study is useful as this small change is sufficient to break the symmetry of the eight equal Schmid factors which characterize the preceding tests with a perfect [0 0 1] compression axis. For the present case, one Schmid factor is larger than all the others at the onset of loading.

The resulting orientation spread during deformation is again, as for the other examples, relatively large (Fig. 10b). However, unlike the other results shown above, the present simulations show a different reorientation tendency. As documented in the inverse pole figure for the case with zero friction conditions (left column in Fig. 10b) the orientation distribution evolves into a pronounced [1 0 1] alignment. This orientation is indeed the most stable orientation for compression of fcc single crystals under pure friction-free compressive loading. However, as in the other cases discussed before, some of the orientation spread observed in this inverse pole figure cannot be attributed to classical Schmid-type orientation evolution owing to the strong inclination of the overall sample shape (Fig. 3). This means that the reference system itself is changed, entailing an overall shift of all orientations in the order of magnitude of the inclination angle between the (new inclined) sample axis and the bottom normal (Figs. 3 and 10a). The two other simulations with a non-zero friction coefficient (middle and right column in Fig. 10a and b) reveal a more homogeneous orientation change towards both the [1 1 1] and the [1 0 1] axis. The sample with a (small) friction coefficient of 0.05 shows a slightly more pronounced tendency of rotations towards [1 0 1] (Fig. 10b).

Concerning the geometrical stability, the present results reveal that a diameter-to-length ratio below 0.4 leads to a pronounced shape instability in all cases studied, irrespective of the initial crystallographic orientation of the compressed specimen. As for the other orientations studied above, non-zero friction conditions generally exert a stabilizing effect on the course of the compression test even when a substantial evolution of orientation scatter takes place.

The stability becomes evident also from the flow curves (Fig. 10c). For the unstable case with zero friction the Considère analysis reveals the onset of instability at an engineering strain of 0.18, which is the smallest for all cases studied. The other two stress–strain curves obtained for non-zero friction conditions remain stable during compression.

4. Conclusions

We have presented crystal plasticity finite element simulations of cylindrical Cu single crystal compression tests. The main parameters were the initial crystallographic orientation, sample geometry (diameter-to-length ratio) and friction. The main results and conclusions are

- Geometrical stability. A diameter-to-length ratio below 0.4 (slim samples) leads to a pronounced shape instability for the stable and unstable orientations inspected. This observation does not match classical isotropic plastic buckling theory but rather resembles an unidirectional bulk shear process of the entire specimen with two main localization zones, one close to the bottom of the pillar and one in the contact zone with the tool. This effect is attributed to the discreteness of the plastic slip in the present crystal plasticity finite element simula-

tion approach. Samples with larger values for the diameter-to-length ratio revealed higher orientation and shape stability during compression.

- Non-zero friction conditions reduce shape instability irrespective of the initial crystallographic orientation of the compressed specimen.
- The initial anisotropy in the form of a different initial crystal orientation has – together with the magnitude of the friction coefficient – an influence on the deformation-induced orientation evolution, its spread and the overall sample shape during compression.
- Pronounced deformation-induced orientation changes including the evolution of substantial orientation gradients (orientation scatter) within the originally homogeneous single crystals takes place already at engineering compressive strains of about 0.2.
- The evolution of orientation scatter during compression within the originally homogeneous single crystals is weaker when the friction coefficient is higher.
- The documented orientation changes during compression may in part be due to changes in the reference system in cases where buckling takes place rather than only to crystallographic reorientations.

Acknowledgements

The authors are grateful for motivating and helpful discussions with R. Maas and H. Van Swygenhoven from the Paul Scherrer Institute (Switzerland) and with M. Uchic and D. Dimiduk from the Air Force Research Laboratory in Dayton, OH (USA).

References

[1] Uchic MD, Dimiduk DM, Florando JN, Nix WD. Sample dimensions influence strength and crystal plasticity. Science 2004;305:986–9.
[2] Greer JR, Oliver WC, Nix WD. Size dependence of mechanical properties of gold at the micronscale in the absence of strain gradients. Acta Mater 2005;53:1821–30.
[3] Nix WD, Greer JR, Feng G, Lilleodden ET. Deformation at the nanometer and micrometer length scales: effects of strain gradients and dislocation starvation. Thin Solid Films, in press.
[4] Dimiduk DM, Uchic MD, Parthasarathy TA. Size affected single slip behavior of pure Ni microcrystals. Acta Mater 2005;53:4065–77.
[5] Volkert CA, Lilleodden ET. Size effects in the deformation of submicro Au columns. Philos Mag 2006;86:5567–79.
[6] Afrin N, Ngan AHW. Creep of micron-sized Ni_3Al columns. Scripta Mater 2006;54:7–12.
[7] Zhang H, Schuster BE, Wei Q, Ramesh KT. The design of accurate micro-compression experiments. Scripta Mater 2005;54:181–6.
[8] Ma A, Roters F, Raabe D. A dislocation density based constitutive model for crystal plasticity FEM including geometrically necessary dislocations. Acta Mater 2006;54:2169–79.
[9] Zaefferer S, Kuo J-C, Zhao Z, Winning M, Raabe D. On the influence of the grain boundary misorientation on the plastic deformation of aluminum bicrystals. Acta Mater 2003;51:4719–35.
[10] Ma A, Roters F, Raabe D. On the consideration of interactions between dislocations and grain boundaries in crystal plasticity finite element modeling – theory, experiments, and simulations. Acta Mater 2006;54:2181–94.
[11] Ma A, Roters F, Raabe D. Studying the effect of grain boundaries in dislocation density based crystal plasticity finite element simulations. Int J Solids Struct 2006;43:7287–303.
[12] Raabe D, Sachtleber M, Zhao Z, Roters F, Zaefferer S. Micromechanical and macromechanical effects in grain scale polycrystal plasticity experimentation and simulation. Acta Mater 2001;49:3433–41.
[13] Wang Y, Raabe D, Klüber C, Roters F. Orientation dependence of nanoindentation pile-up patterns and of nanoindentation microtextures in copper single crystals. Acta Mater 2004;52:2229–38.
[14] Zaafarani N, Raabe D, Singh RN, Roters F, Zaefferer S. Three dimensional investigation of the texture and microstructure below a nanoindent in a Cu single crystal using 3D EBSD and crystal plasticity finite element simulations. Acta Mater 2006;54:1707–994.
[15] Rice JR. Inelastic constitutive relations for solids: an internal variable theory and its application to metal plasticity. J Mech Phys Sol 1971;19:433–55.
[16] Peirce D, Asaro RJ, Needleman A. An analysis of nonuniform and localized deformation in ductile single crystals. Acta Metall 1982;30:1087–119.
[17] Peirce D, Asaro RJ, Needleman A. Material rate dependence and localized deformation in crystalline solids. Acta Metall 1983;31:1951–76.
[18] Raabe D, Roters F, Barlat F, Chen L-Q, editors. Continuum Scale Simulation of Engineering Materials. Weinheim: Wiley-VCG; 2004, ISBN 3-527-30760-5.
[19] Kalidindi SR, Bronkhorst CA, Anand L. Crystallographic texture evolution in bulk deformation processing of FCC metals. Mech Phys Solids 1992;40:537–69.
[20] Raabe D, Roters F. Using texture components in crystal plasticity finite element simulations. Int J Plast 2004;20:339–61.
[21] Hutchinson JW. Bounds and self-consistent estimates for creep of polycrystalline materials. Proc Roy Soc A 1976;348:101–27.
[22] MSC. Marc user manual, Vol. D, MSC Software Corporation, 2001.
[23] Raabe D, Zhao Z, Park S-J, Roters F. Theory of orientation gradients in plastically strained crystals. Acta Mater 2002;50:421–40.
[24] Raabe D, Zhao Z, Roters F. Study on the orientational stability of cube-oriented FCC crystals under plane strain by use of a texture component crystal plasticity finite element method. Scripta Mater 2004;50:1085–90.